


First-principles estimation of the superconducting transition temperature of a metallic hydrogen liquid

Haoran Chen,¹ Xiao-Wei Zhang¹,,¹ Xin-Zheng Li,² and Junren Shi^{1,3,*}

¹International Center for Quantum Materials, Peking University, Beijing 100871, China

²State Key Laboratory for Artificial Microstructure and Mesoscopic Physics, and School of Physics, Peking University, Beijing 100871, China

³Collaborative Innovation Center of Quantum Matter, Beijing 100871, China



(Received 3 August 2021; revised 18 October 2021; accepted 15 November 2021; published 24 November 2021)

We present a full density-functional theory-based implementation of the stochastic path-integral approach proposed by Liu *et al.* [H. Liu, Y. Yuan, D. Liu, X.-Z. Li, and J. Shi, *Phys. Rev. Research* **2**, 013340 (2020)] for estimating the superconducting transition temperature (T_c) of a liquid. The implementation is based on the all-electron projector augmented-wave (PAW) method. We generalize Liu *et al.*'s formalism to accommodate the pseudodescription of electron states in the PAW method. A formula for constructing the overlap operator of the PAW method is proposed to eliminate errors due to the incompleteness of a pseudobasis set. We apply the implementation to estimate T_c 's of metallic hydrogen liquids. It confirms Liu *et al.*'s prediction that metallic hydrogen could form a superconducting liquid.

DOI: [10.1103/PhysRevB.104.184516](https://doi.org/10.1103/PhysRevB.104.184516)

I. INTRODUCTION

Ever since the discovery of the superconductivity by K. Onnes in 1911, the search for materials with high superconducting transition temperatures (T_c 's) has been a constant pursuit. The recent discovery of a new family of high- T_c superconductors in hydrides under high pressure shows the great promise of first-principles calculations in guiding the search [1,2]. Based on the celebrated Bardeen-Cooper-Schrieffer (BCS) theory of superconductivity, it was long predicted that metallic hydrogen or hydrogen-rich materials could exhibit high T_c 's as light hydrogen atoms provide both a high Debye frequency of phonons and a strong electron-phonon coupling (EPC) [3–6]. By using state-of-the-art first-principles approaches based on the density-functional theory (DFT), it is now possible to conduct an extensive search in various hydrides, and predict their structures and T_c 's [1,2,7–9].

In spite of the tremendous success, the first-principles prediction of T_c for compounds like hydrides is tricky. The widely adopted algorithm is based on the Eliashberg theory which relates T_c to quantities calculable by DFT such as the band structure of electrons and the matrix elements of EPC [10,11]. The theory is built on the assumption that the vibration amplitudes of atoms in a solid are small. It thus adopts the harmonic approximation for describing atom vibrations and a perturbative approach for determining EPC effects. In hydrides, however, the assumption likely breaks down. Light hydrogen atoms tend to have large vibration amplitudes, and, therefore, their vibrations are subject to anharmonicity [12]. Moreover, hydrogen atoms can tunnel between lattice sites and could even form a superionic phase in which they become

delocalized and diffuse in a whole lattice [13]. In the mother compound of metallic hydrides, i.e., metallic hydrogen, quantum fluctuations induced by the tunneling is so strong that its melting point is predicted to be suppressed below room temperature [14,15]. The applicability of the Eliashberg theory in these systems is questionable.

To date, most of the efforts addressing the quantum tunneling and anharmonic effects in superconductors are based on the approach of the stochastic self-consistent harmonic approximation (SSCHA) [16] which treats an anharmonic system as an effective harmonic one with self-consistently determined phonon modes. T_c can then be estimated by applying the standard algorithm for a harmonic system. SSCHA calculations show that the anharmonicity and quantum fluctuations could yield different predictions of crystal structures and T_c 's [12,17]. While the approach is effective and efficient, it relies on a cascade of approximations which could become uncontrolled. In particular, when a system enters a liquid or superionic phase, the underlying assumption that the system can be approximated as a harmonic solid obviously breaks down.

Recently, Liu *et al.* proposed a stochastic path-integral approach of determining T_c for general systems including liquids [18]. The core of the approach is a set of rigorous relations through which an effective pairing interaction between electrons can be inferred from the fluctuations of electron-ion-scattering \mathcal{T} matrices. The fluctuations of the \mathcal{T} matrices can be estimated from a stochastic sampling of ion positions generated by a path-integral molecular dynamics (PIMD) simulation [19]. Furthermore, it is shown that the equations for determining T_c in the Eliashberg theory, i.e., the linearized Eliashberg equations, can be reestablished rigorously in the new context. As a result, with the effective pairing interaction, T_c can be determined in the exactly same manner as in the

*junrenshi@pku.edu.cn

conventional Eliashberg approach. The approach is based on a rigorous theory and makes no assumption on the nature of atom motion. It should, therefore, apply equally well for solids or liquids with or without anharmonicity and quantum fluctuations.

Liu *et al.* present an implementation of the approach for metallic hydrogen liquids in Ref. [18]. They predict that metallic hydrogen would form a superconducting liquid with T_c well above its melting temperature. In the implementation, hydrogen atom positions are sampled by using the first-principles PIMD method. However, ionic fields, i.e., the interaction potentials between hydrogen ions and electrons, are approximated as a bare Coulomb potential screened by a dielectric function. Such a linear screening approximation (LSA) should be adequate for metallic hydrogen because hydrogen ions, i.e., protons, are point particles without inner-core electrons. For more general systems involving other atom species as in the case of hydrides, however, the approximation is obviously inadequate. The deficiency limits the applicability of the implementation to metallic hydrogen only.

In this paper, we develop a full DFT-based implementation of the stochastic path-integral approach for determining T_c . We base our implementation on the Vienna Ab-initio Simulation Package (VASP) [20,21] and determine ionic fields by employing the projector augmented-wave (PAW) method [22,23]. In the method, the states of valance electrons are described by pseudo (PS)-wave functions and the all-electron (AE) wave functions, i.e., the true wave functions of electrons are related to PS-wave functions through a transformation that depends on the positions of ions. It thus introduces complexities in directly applying Liu *et al.*'s formalism. We solve the issue by generalizing the formalism and accommodating it to the PS description. The generalized formalism enables our full DFT-based implementation. As a test, we apply the implementation to metallic hydrogen liquids. It yields results close to Liu *et al.*'s results, confirming the prediction that metallic hydrogen could form a superconducting liquid.

The remainder of the paper is organized as follows. In Sec. II, we outline the formalism and calculation procedure of the stochastic path-integral approach proposed by Liu *et al.* and identify main approximations in their implementation. In Sec. III, we generalize and implement Liu *et al.*'s formalism to accommodate the PAW method. A number of issues relevant to the implementation are also addressed. In particular, a formula for constructing the overlap operator in the PAW method is proposed to eliminate errors due to the incompleteness of the PS basis set. In Sec. IV B, we apply the implementation to metallic hydrogen liquids and compare results with Liu *et al.*'s results. The convergency of the calculation is also tested. Finally, we summarize our results in Sec. V.

II. STOCHASTIC PATH-INTEGRAL APPROACH OF DETERMINING T_c

In this section, we outline the formalism of the stochastic path-integral approach of determining T_c proposed by Liu *et al.* and discuss approximations involved in implementing the approach.

A. Formalism

In the conventional Eliashberg theory, T_c is determined by solving a set of linearized Eliashberg equations. Liu *et al.* show rigorously that the same set of equations still hold for liquids and general systems, provided that relevant parameters are properly determined. The set of the linearized Eliashberg equations reads

$$\rho \Delta_n = \sum_{n'} \left[\lambda(n' - n) - \mu^* - \frac{\hbar\beta}{\pi} |\tilde{\omega}(n)| \delta_{nn'} \right] \Delta_{n'}, \quad (1)$$

$$\tilde{\omega}(n) = \frac{\pi}{\hbar\beta} \left(2n + 1 + \lambda(0) + 2 \sum_{m=1}^n \lambda(m) \right), \quad n \geq 0 \quad (2)$$

and $|\tilde{\omega}(-n)| = |\tilde{\omega}(n-1)|$, where n and n' are integers indexing the Matsubara frequencies of fermions $\omega_n = (2n + 1)\pi/\hbar\beta$, $\beta \equiv 1/k_B T$ and T is the temperature; $\{\lambda(m), m \in \mathbb{Z}\}$ is a set of interaction parameters characterizing the effective pairing interaction, and μ^* is the empirical Morel-Anderson pseudopotential introduced to take account of the exchange-correlation effect of electrons [24]. Solving Eq. (1) yields a set of eigenvalues ρ and eigenvectors Δ_n . For normal states, all eigenvalues are negative. The emergence of a nonnegative eigenvalue indicates that the system enters into the superconducting state. One can thus estimate T_c by solving the equations for a number of temperatures to see when the maximal eigenvalue changes sign. We note that Δ_n here is not related to the physical gap.

Two comments are in order. First, in calculations for solids using the standard approach (see, e.g., Ref. [6]), it is common to use the empirical McMillan formula and estimate T_c from a small number of parameters evaluated at zero temperature including the mass enhancement factor $\lambda \equiv \lambda(0)$, an average phonon frequency, and μ^* . It simplifies the calculations. Unfortunately, such an approach does not work well for liquids because (a) unlike harmonic solids, λ and the average phonon frequency of a liquid are temperature dependent; (b) the empirical formulas are tuned for solids and do not fit well with liquids which have qualitatively different density spectral functions due to the presence of low-frequency diffusive modes [25,26]. Second, the choice of parameter μ^* is empirical. For metallic hydrogen systems, we use $\mu^* \approx 0.089$ as suggested in Ref. [6]. The empirical parameter introduces an uncertainty in predicting T_c . Ideally, one should base calculations on the DFT for superconductors [27–29], which provides a rigorous framework for treating exchange-correlation effects in superconductors. This is not yet implemented in our current calculation.

To apply the Eliashberg equations, the interaction parameters $\lambda(m)$ are the central quantities to be determined. They are related to the effective pairing interaction W by

$$\lambda(n - n') = - \sum_{\mathbf{k}'} W(\omega_n - \omega_{n'}, \mathbf{k} - \mathbf{k}') \delta(\tilde{\epsilon}_{\mathbf{k}'} - \epsilon_F), \quad (3)$$

where $W(\omega_n - \omega_{n'}, \mathbf{k} - \mathbf{k}')$ denotes the matrix element of the effective pairing interaction, which is a function of the quasi-wave-vector transfer $\mathbf{k} - \mathbf{k}'$ and the frequency transfer $\omega_n - \omega_{n'}$, $\tilde{\epsilon}_{\mathbf{k}'}$ is the renormalized quasielectron dispersion, and ϵ_F is the Fermi energy. To apply the formula, it is necessary

to determine the effective pairing interaction as well as the renormalized quasielectron dispersion.

To determine these quantities in a liquid, Liu *et al.* propose a stochastic path-integral approach. It is based on the classical isomorphism [30], i.e., mapping quantum ions to classical ring polymers by applying the imaginary-time path-integral formalism [31]. The spatial configuration of the classical ensemble of ring polymers is specified by a set of τ -dependent coordinates $\{\mathbf{R}_a(\tau)\}$, where $\tau \in [0, \hbar\beta)$ is the imaginary time or interpreted as a variable to parametrize the rings. In a PIMD simulation, the isomorphic ensemble is simulated by using the classical molecular dynamics. It provides a statistical sampling of the spatial configurations of the ring polymers.

Quantities related to electrons can be evaluated in the isomorphic ensemble. Electrons in the ensemble experience a τ -dependent Kohn-Sham (KS) potential $V_{\text{KS}}(\tau)$ which is self-consistently determined by the ion configuration $\{\mathbf{R}_a(\tau)\}$ at the specific imaginary-time τ . As a result, the single-particle Green's function of electrons with respect to a given configuration of ring polymers, in the context of the KS theory, can be determined by

$$\left[-\frac{\partial}{\partial \tau} - \frac{\hat{H}(\tau) - \epsilon_F \hat{\mathbb{1}}}{\hbar} \right] \hat{\mathcal{G}}(\tau, \tau') = \delta(\tau - \tau') \hat{\mathbb{1}}, \quad (4)$$

where we write the equation in an operator form, $\hat{H}(\tau) \equiv \hat{K} + \hat{V}_{\text{KS}}(\tau)$ with \hat{K} being the operators of the kinetic energy. The Green's function is not a physical Green's function for electrons in a liquid. To get the physical one, we need to further conduct an ensemble average:

$$\mathcal{G}_{\text{phy.}} \equiv \bar{\mathcal{G}}(\tau - \tau') = \langle \mathcal{G}(\tau, \tau') \rangle_C, \quad (5)$$

where $\langle \dots \rangle_C$ denotes the average over the ring-polymer configurations. The averaged (physical) Green's function $\bar{\mathcal{G}}(\tau - \tau')$ defines the dispersion and lifetime of a quasielectron renormalized by the fluctuating ionic field. The quasielectron dispersion $\tilde{\epsilon}_{\mathbf{k}}$ required by Eq. (3) can then be inferred from it.

For a given spatial configuration of ring polymers, we can determine the electron-ion-scattering \mathcal{T} matrix. The \mathcal{T} matrix is related to the Green's function according to the Lippmann-Schwinger equation

$$\hat{\mathcal{T}} = \hat{\mathcal{V}} + \frac{1}{\hbar} \hat{\mathcal{V}} \hat{\mathcal{G}} \hat{\mathcal{T}}, \quad (6)$$

where $\hat{\mathcal{V}} = \hat{V}_{\text{KS}}(\tau) - \hat{\Sigma}$ is the effective scattering potential for electrons, and $\hat{\Sigma}$ is the self-energy inferred from $\hat{\mathcal{G}}$.

Liu *et al.* establish a rigorous relation between the effective pairing interaction and the \mathcal{T} matrices. One first determines the pair-scattering amplitude Γ , i.e., the fluctuation of the \mathcal{T} matrices:

$$\Gamma_{11'} = -\beta \langle |\mathcal{T}_{11'}|^2 \rangle_C, \quad (7)$$

where $\mathcal{T}_{11'}$ denotes the matrix element of the \mathcal{T} matrix, and we adopt a short-hand notation by using \mathbf{n} and $\bar{\mathbf{n}}$ to represent the states of electrons: $\mathbf{1} \equiv (\mathbf{k}, \omega_n)$, $\bar{\mathbf{1}} \equiv (-\mathbf{k}, -\omega_n)$ and similarly for $1'$ and $\bar{1}'$. Then, the effective pairing interaction can be obtained by solving the Bethe-Salpeter equation:

$$W_{11'} = \Gamma_{11'} + \frac{1}{\hbar^2 \beta} \sum_2 \Gamma_{12} |\bar{\mathcal{G}}_2|^2 W_{21'}. \quad (8)$$

The obtained $W_{11'}$ then enters into Eq. (3), in which we express it explicitly as $W_{11'} \equiv W(\omega_n - \omega_{n'}, \mathbf{k} - \mathbf{k}')$. We note that in general $W_{11'}$ depends on 1 and $1'$ independently. For EPC, it is a good approximation to regard $W_{11'}$ as a function of $\omega_n - \omega_{n'}$ as long as $\hbar|\omega_{n(n')}|$ is much smaller than the Fermi energy. Moreover, since liquids are isotropic and only matrix elements with both \mathbf{k} and \mathbf{k}' residing on the Fermi surface are needed for evaluating Eq. (3), $W_{11'}$ can be written as a function of $\mathbf{k} - \mathbf{k}'$.

B. Approximations

To develop an algorithm for estimating T_c based on the rigorous formalism shown in the last subsection, Liu *et al.* employ a number of approximations. In this subsection, we will discuss these approximations and identify the one to be improved.

The most important approximation which makes an implementation possible is the quasistatic approximation. It is necessary because solving Eqs. (4) and (22) exactly is deemed to be impossible in practice as it requires a time resolution $\sim \hbar/\epsilon_F$ or a corresponding large cutoff frequency $\sim \epsilon_F/\hbar$. Fortunately, one can exploit the fact that ions move much slower than electrons. It means that the ionic field only has significant components for frequencies $\nu_m \equiv 2\pi m/\hbar\beta \lesssim \omega_{\text{ph}}$, where ω_{ph} is a characteristic frequency of phonons. In this case, the equation can be solved by applying the quasistatic approximation. This is to choose a large n such that $\omega_n \gg \omega_{\text{ph}}$ and to solve Eq. (4) as if $\hat{H}(\tau)$ is time independent:

$$\hat{\mathcal{G}}_n(\tau) = \hbar[(i\hbar\omega_n + \epsilon_F)\hat{\mathbb{1}} - \hat{H}(\tau)]^{-1}, \quad (9)$$

The ensemble average $\hat{\mathcal{G}}_n = \langle \hat{\mathcal{G}}_n(\tau) \rangle_C$ will be independent of τ and a good approximation for the Fourier transform of $\bar{\mathcal{G}}(\tau - \tau')$ at the frequency ω_n [18]. The \mathcal{T} matrix can then be calculated in the time domain in the same manner and Fourier transformed back to the frequency domain; see Sec. III B for details. For determining the effective pairing potential, we only need to solve for a specific n with $\omega_{\text{ph}} \ll \omega_n \ll \epsilon_F/\hbar$. This is because $W_{11'} \equiv W(\omega_n - \omega_{n'}, \mathbf{k} - \mathbf{k}')$ is assumed to be a function of $\omega_n - \omega_{n'} \equiv \nu_m$.

More approximations are involved in PIMD simulations. It is necessary to simulate a system in a finite size supercell and discretize the imaginary time to a finite number of beads. In Ref. [18] it is found that the discretization truncates the high-frequency components of the density correlation function of ions and the effective pairing interaction. It results in an incorrect asymptotic behavior of $\lambda(m)$ at large m . To address the issue, Liu *et al.* develop an oversampling scheme to interpolate the density correlation function in the temporal domain and obtain an oversampled density correlation function; see Ref. [18] for details. To get the effective pairing interaction, they make use of the empirical relation:

$$W(\nu_m, \mathbf{q}) = |M(\nu_m, \mathbf{q})|^2 \chi(\nu_m, \mathbf{q}), \quad (10)$$

where $\chi(\nu_m, \mathbf{q})$ is the density correlation function of ions, and $M(\nu_m, \mathbf{q})$ could be regarded as the EPC matrix element as defined in the Eliashberg theory. It is found numerically that the relation holds well for metallic hydrogen liquids, and $|M(\nu_m, \mathbf{q})|^2$ can be obtained from a linear regression. By substituting the density correlation function in Eq. (10) with the oversampled one, one can obtain an oversampled effective

pairing interaction. It is found that $\lambda(m)$ determined from the oversampled effective pairing interaction has a correct asymptotic behavior at large m .

Last, Liu *et al.* adopt the LSA for evaluating the ionic field. This is to approximate the Fourier transform of the ionic potential as

$$V_{\text{ion}}(\mathbf{q}, \tau) = \frac{e^2}{\varepsilon_{\text{et}}(\mathbf{q})q^2} \rho_i(\mathbf{q}, \tau), \quad (11)$$

where $\rho_i(\mathbf{q}, \tau) = \sum_a \exp[-i\mathbf{q} \cdot \mathbf{R}_a(\tau)]$ is the Fourier transform of the density distribution of ions, and $\varepsilon_{\text{et}}(\mathbf{q})$ is the static electron-test charge dielectric function [32] which has a form similar to that of the random-phase approximation but with a local-field correction factor determined by Ichimaru and Utsumi [33]. It is derived from the jellium model which models ions as a uniform positive charge background, an approximation which obviously breaks down in core regions close to ions. While it is reasonable to expect that such an approximation could work well for metallic hydrogen in which ions (protons) have small core volumes and electrons are shared by all ions, it becomes problematic when other atoms are involved and bonding between atoms is covalent in nature.

Among the three approximations, the LSA is the one that severely limits the applicability of Liu *et al.*'s implementation for systems other than metallic hydrogen. This will be the focus of this paper aiming to improve the implementation. The effect of the finite simulation supercell and the finite number of beads should be assessed to make sure that calculations converge. This will also be tested. Finally, it is the quasistatic approximation which makes an implementation feasible for EPC. The approximation is valid because phonons have an energy scale much smaller than that of electrons, a feature unique to conventional EPC superconductors.

III. FORMALISM FOR THE PAW METHOD

In this section, we develop formalism for a full DFT-based implementation. To balance speed and accuracy, we base our implementation on the PAW method [22,23]. As a pseudopotential method, the PAW method is efficient. Meanwhile, one can obtain AE wave functions from PS wave functions by applying a transformation. The latter is particularly useful for us since the formalism presented in Sec. II is established in an AE basis. To facilitate an implementation based on the PAW method, we need formulas of determining the AE Green's functions and the \mathcal{T} matrices by using quantities defined in the PS basis.

In Sec. III A, we first briefly review the PAW method and outline its formalism. With the preparation, we derive formulas for determining the AE Green's functions and the \mathcal{T} matrices by using the PAW method in Sec. III B. In Sec. III C, we discuss the evaluations of quantities involved in the formulas, including the transformation matrix and the overlap matrix.

A. PAW method

In the PAW method, electrons are described by PS wave functions. A transformation operator is introduced to map a

PS wave-function $\tilde{\Psi}$ to an AE wave-function Ψ :

$$\Psi = \hat{T}\tilde{\Psi} \equiv \tilde{\Psi} + \sum_a \hat{T}^a |\tilde{\Psi}\rangle, \quad (12)$$

where \hat{T}^a is an operator transforming the core state of the ion a from the PS space to the AE space and is nonzero only within an augmentation sphere surrounding the ion. The radius of the sphere is chosen such that there is no overlap between spheres associated with different ions. Inside a sphere, the wave functions are expanded in the basis of partial waves:

$$\hat{T}^a |\tilde{\Psi}\rangle = |\Psi^a\rangle - |\tilde{\Psi}^a\rangle = \sum_i (|\phi_i^a\rangle - |\tilde{\phi}_i^a\rangle) |\tilde{p}_i^a\rangle |\tilde{\Psi}\rangle, \quad (13)$$

where i indexes the partial-wave states with angular-momentum quantum numbers $(l_i m_i)$ and at a given reference energy ϵ_i . The AE partial-wave-functions $\langle \mathbf{r} | \phi_i^a \rangle \equiv \phi_{l_i \epsilon_i}^a(r) Y_{l_i m_i}(\hat{\mathbf{r}})$ at the radial coordinate r and along the direction $\hat{\mathbf{r}}$ are obtained by solving a spherical AE Schrodinger equation at the reference energy in the presence of an ion at the center. The corresponding PS partial-wave-functions $\langle \mathbf{r} | \tilde{\phi}_i^a \rangle$ are chosen such that they are smooth and coincide with the AE partial-wave functions outside the sphere; $|\tilde{p}_i^a\rangle$ are a set of projectors that are biorthogonal to the PS partial-wave states:

$$\langle \tilde{p}_j^a | \tilde{\phi}_i^a \rangle = \delta_{i,j}. \quad (14)$$

With a complete set of the basis, the closure relation in each sphere can be written as:

$$\sum_i |\tilde{\phi}_i^a\rangle \langle \tilde{p}_i^a| = \hat{\mathbb{I}}^a. \quad (15)$$

In the PS basis, the KS equation is transformed to

$$\hat{H} \tilde{\Psi}_n = \epsilon_n \hat{S} \tilde{\Psi}_n, \quad (16a)$$

$$\hat{H} = \hat{T}^\dagger \hat{H} \hat{T}, \quad (16b)$$

$$\hat{S} = \hat{T}^\dagger \hat{T}, \quad (16c)$$

where \hat{H} and \hat{H}^\dagger denote the Hamiltonians in the AE and PS basis, respectively. This is a generalized eigenvalue problem, and the orthogonality condition between PS eigenwave functions becomes

$$\langle \tilde{\Psi}_m | \tilde{\Psi}_n \rangle = \langle \tilde{\Psi}_m | \hat{S} | \tilde{\Psi}_n \rangle = \delta_{m,n}. \quad (17)$$

We note that in DFT calculations based on the PAW method, the PS Hamiltonian is directly derived from a total-energy functional expressed in terms of the PS wave functions. It is not necessary to construct the AE Hamiltonian first and then transform it to the PS Hamiltonian by using Eq. (16b).

B. AE Green's function and \mathcal{T} -matrix

With the preparation, we now proceed to derive formulas for determining the AE Green's function and the \mathcal{T} matrix by using the PAW method.

We seek for an expression of the Green's function appropriate for the PAW method. Under the quasistatic approximation, the AE Green's function is determined by Eq. (9). However, it depends on the AE Hamiltonian $\hat{H}(\tau)$. We can transform it to a form that only depends on quantities in the PS basis. To

see that, we start from the spectral representation of a general Green's function $\hat{G}(\epsilon) = \hbar(\epsilon\hat{\mathbb{1}} - \hat{H})^{-1}$:

$$\hat{G}(\epsilon) = \hbar \sum_n \frac{|\Psi_n\rangle\langle\Psi_n|}{\epsilon - \epsilon_n} = \hat{T} \left[\hbar \sum_n \frac{|\tilde{\Psi}_n\rangle\langle\tilde{\Psi}_n|}{\epsilon - \epsilon_n} \right] \hat{T}^\dagger, \quad (18)$$

where $|\Psi_n\rangle$ and $|\tilde{\Psi}_n\rangle$ are the AE and PS eigenwave functions, respectively, and ϵ_n is the corresponding eigenenergy.

We can convert the expression to a more convenient form. By using the orthonormality condition Eq. (17), it is easy to verify the closure relation

$$\sum_n \hat{S} |\tilde{\Psi}_n\rangle\langle\tilde{\Psi}_n| = \hat{\mathbb{1}}. \quad (19)$$

We then have

$$\begin{aligned} (\epsilon\hat{S} - \hat{H})^{-1} &= \sum_n (\epsilon\hat{S} - \hat{H})^{-1} \hat{S} |\tilde{\Psi}_n\rangle\langle\tilde{\Psi}_n| \\ &= \sum_n \frac{|\tilde{\Psi}_n\rangle\langle\tilde{\Psi}_n|}{\epsilon - \epsilon_n}, \end{aligned} \quad (20)$$

where we make use of the eigen equation Eq. (16a). By substituting the equality into Eq. (18) and setting $\epsilon = i\hbar\omega_n + \epsilon_F$, we obtain the formula of determining the AE Green's function in the PAW method:

$$\hat{G}_n(\tau) = \hbar\hat{T}(\tau)[(i\hbar\omega_n + \epsilon_F)\hat{S}(\tau) - \hat{H}(\tau)]^{-1}\hat{T}^\dagger(\tau). \quad (21)$$

We note that \hat{H} , \hat{S} , and \hat{T} all depend on the configuration of ions and are, therefore, time dependent.

With the Green's function, the scattering \mathcal{T} matrix can be determined. To avoid solving the Lippmann-Schwinger equation in the AE space, we apply an identity

$$\hat{\mathcal{T}}_n(\tau) = \hbar\hat{\mathcal{G}}_n^{-1}\hat{G}(\tau)\hat{\mathcal{G}}_n^{-1} - \hbar\hat{\mathcal{G}}_n^{-1} \quad (22)$$

to calculate the \mathcal{T} matrix in time domain. It is easy to prove that the \mathcal{T} matrix calculated in this way satisfies Eq. (6). We note that in a liquid, because of the spatial translation symmetry, the average Green's function is diagonal in the plane-wave basis. As a result, the matrix inverse and multiplication can be carried out in a truncated Hilbert space spanned by the basis without introducing errors.

The matrix elements of \mathcal{T} matrix in the frequency domain can then be determined by applying the Fourier transform:

$$\hat{\mathcal{T}}_{\omega_n + \nu_m, \omega_n} \approx \frac{1}{\hbar\beta} \int_0^{\hbar\beta} d\tau \hat{\mathcal{T}}_n(\tau) e^{i\nu_m\tau}. \quad (23)$$

The matrix elements are all that are needed for evaluating the pair-scattering amplitude and the effective pairing interaction (see Sec. II A). We note that for the purpose only, the matrix elements with wave vectors close to the Fermi surface are needed. Therefore, a large energy cutoff, which is required for recovering the AE wave functions from the PS wave functions, is not needed for our calculation.

C. Transformation and overlap matrices

To apply the formulas derived in the last subsection, it is necessary to determine the transformation operator \hat{T} and the overlap matrix \hat{S} .

The transformation operator transforms a PS state to an AE state. From Eq. (12) and Eq. (13), the operator is

$$\hat{T} = \hat{\mathbb{1}} + \sum'_{j,a} (|\phi_j^a\rangle - |\tilde{\phi}_j^a\rangle)\langle\tilde{p}_j^a|, \quad (24)$$

where the summation is over ions and partial waves, with the prime indicating explicitly that the summation is always truncated to a small number of partial waves in real calculations. For liquids, the basis states in both the AE space and the PS space are the plane waves. A matrix element in the plane-wave basis is

$$\langle\psi_k|\hat{T}|\tilde{\psi}_{k'}\rangle = \delta_{kk'} + \sum'_{i,a} (\langle\psi_k|\phi_i^a\rangle - \langle\psi_k|\tilde{\phi}_i^a\rangle)\langle\tilde{p}_i^a|\tilde{\psi}_{k'}\rangle, \quad (25)$$

where $|\psi_k\rangle$ and $|\tilde{\psi}_{k'}\rangle$ are the plane waves in the AE and PS space, respectively. The overlap matrix element between a plane wave and a partial wave can be evaluated by

$$\langle\psi_k|\phi_i^a\rangle = \frac{4\pi}{\sqrt{V}} e^{-ik\cdot\mathbf{R}_a} Y_{l,m_i}(\hat{\mathbf{k}}) \int_0^{r_c} r^2 dr (-i)^l j_l(kr) \phi_{l,m_i}^a(r), \quad (26)$$

and similarly for other matrix elements, where Y_{lm} denotes the spherical harmonics, $j_l(kr)$ is the spherical Bessel function, r_c denotes the cutoff radius of the augmentation sphere in defining \hat{T}^a , and \mathbf{R}_a is the position of the ion a .

The overlap matrix $\hat{S} = \hat{T}^\dagger\hat{T}$ can also be determined by using the partial waves. From Eq. (24), we have

$$\begin{aligned} \hat{S} &= -\hat{\mathbb{1}} + \hat{T} + \hat{T}^\dagger \\ &+ \sum'_{ij,a} |\tilde{p}_i^a\rangle\langle\phi_i^a - \tilde{\phi}_i^a| \langle\phi_j^a - \tilde{\phi}_j^a|\langle\tilde{p}_j^a|, \end{aligned} \quad (27)$$

where we assume that augmentation spheres associating with different ions do not overlap. We can rewrite it as

$$\hat{S} = \hat{S}' + (\hat{T} - \hat{T}' + \text{H.c.}), \quad (28)$$

where

$$\hat{S}' = \hat{\mathbb{1}} + \sum'_{ij,a} |\tilde{p}_i^a\rangle\langle(\phi_i^a|\phi_j^a) - \langle\tilde{\phi}_i^a|\tilde{\phi}_j^a\rangle\langle\tilde{p}_j^a|, \quad (29)$$

$$\hat{T}' = \hat{\mathbb{1}} + \sum'_{ij,a} |\tilde{p}_j^a\rangle\langle(\tilde{\phi}_j^a|\phi_i^a) - \langle\tilde{\phi}_j^a|\tilde{\phi}_i^a\rangle\langle\tilde{p}_i^a|. \quad (30)$$

We note that \hat{S}' is the form commonly adopted in the literature. Actually, by using the closure relation Eq. (15), it is easy to see that \hat{T}' is equal to \hat{T} , and therefore $\hat{S} = \hat{S}'$ if the summation is over a complete set of partial waves. However, since real calculations always use just a small set of partial waves instead of a complete set, the correction due to $\hat{T} - \hat{T}'$ could be non-negligible. For the determination of the AE Green's function and the \mathcal{T} matrix, it is important to maintain the consistency between \hat{T} and \hat{S} since they both appear in Eq. (21). For this reason, we use Eq. (28) instead of Eq. (29) for calculating the overlap matrix.

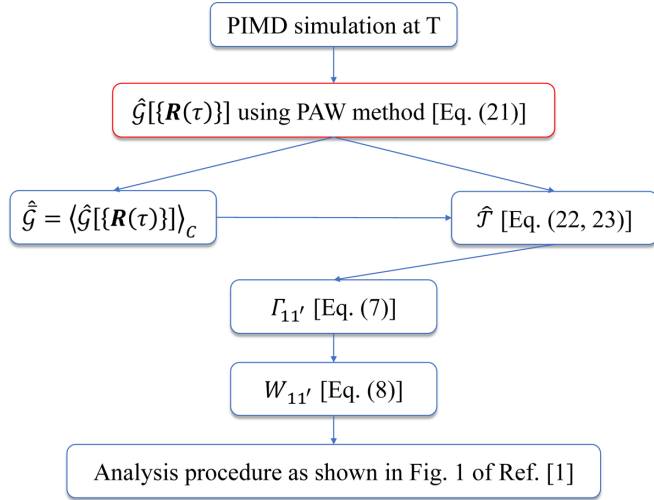


FIG. 1. Flowchart for calculating Green's function and the \mathcal{T} matrix. It substitutes the corresponding part of the workflow shown in Fig. 1 of Ref. [18].

IV. IMPLEMENTATION AND RESULTS

A. Implementation

We employ the GPU version of VASP [34,35] for calculating electron structures. The radius of the augmentation spheres is set to 0.52 Å, which may result in overlaps of the spheres in some ionic configurations but saves computation time. We test a smaller radius of 0.43 Å and find that differences in calculation results are negligible. The Perdew-Burke-Ernzerhof (PBE) exchange-correlation functional [36] is used in all calculations. A Monkhorst-Pack k-point mesh of spacing not larger than $2\pi \times 0.05 \text{ \AA}^{-1}$ is used to sample the Brillouin zone, and an energy cutoff of 600 eV is employed to

expand the wave functions, yielding a convergence in energy better than $\sim 2 \text{ meV/atom}$.

To determine the Green's function and the scattering \mathcal{T} matrix by using Eqs. (21, 22), we need to obtain the pseudo-Hamiltonian \hat{H} , the transformation matrix \hat{T} , and the overlap matrix \hat{S} from the electron structure calculations. Since VASP does not calculate or output these quantities directly, we modify it to output intermediate quantities including the local part of the effective KS potential \tilde{v}_{loc} , the coefficients of the nonlocal part of the effective KS potential $(\tilde{v}')_{ij}^a$, as well as the projector matrix elements $\langle \tilde{\psi}_k | \tilde{p}_i^a \rangle$. With them, the matrix elements $\langle \tilde{\psi}_k | \hat{H} | \tilde{\psi}_{k'} \rangle$ of the pseudo-Hamiltonian can be determined by using the definition

$$\hat{H} = \hat{K} + \tilde{v}_{\text{loc}} + \sum_{ij,a} |\tilde{p}_i^a\rangle (\tilde{v}')_{ij}^a \langle \tilde{p}_j^a|. \quad (31)$$

The matrix elements of the transformation operators \hat{T} , \hat{T}' and the overlap matrix \hat{S}' can also be determined by applying Eq. (24), Eq. (30), and Eq. (29), respectively. It is then straightforward to determine \hat{S} by applying Eq. (28).

We can then proceed to carry out the analysis outlined in Sec. II by following the procedure detailed in Ref. [18]. Figure 1 shows the flowchart of our implementation.

B. Results

To test our first-principles implementation based on the PAW method, we apply it to metallic hydrogen liquids. The ion configurations from the constant-volume PIMD simulations of 200 hydrogen atoms in Ref. [18] are reused in the current study. In this subsection, we summarize our calculation results.

Estimated T_c 's as well as relevant parameters of metallic hydrogen liquids under pressures from 0.5 to 1.5 TPa are

TABLE I. Mass enhancement factor $\lambda \equiv \lambda(0)$, average phonon frequency $\bar{\omega}_2$ (in meV), and the maximal eigenvalue ρ_m of the linearized Eliashberg equations for different pressures P (in TPa) and temperatures T (in K), determined by the standard first-principles approach (PAW method) and the LSA.^a The transition temperature T_c , i.e., the temperature at which ρ_m becomes zero, is estimated based on a linear interpolation of ρ_m between the two temperatures. Numerical uncertainties of the quantities are indicated in parentheses.

		r_s	1.226	1.197	1.17	1.149	1.113	1.049	
		P	0.5	0.6	0.7	0.8	1.0	1.5	
PAW method	350K	λ	10.2(15)	9.0(10)	8.5(10)	7.5(9)	6.3(8)	5.2(5)	
		$\bar{\omega}_2$	102.1(10)	110.9(10)	112.2(15)	124.6(7)	134.6(3)	164.1(30)	
		ρ_m	0.37(12)	0.36(11)	0.32(10)	0.31(9)	0.32(11)	0.26(9)	
	450K	λ	8.2(16)	7.7(10)	7.1(8)	6.3(10)	5.5(6)	4.6(4)	
		$\bar{\omega}_2$	115.0(1)	114.9(13)	132.0(7)	141.9(4)	147.3(11)	173.1(12)	
		ρ_m	-0.10(12)	-0.13(9)	-0.13(8)	-0.10(10)	-0.14(7)	-0.14(6)	
		T_c	428(25)	423(19)	421(19)	425(24)	420(19)	415(17)	
	Linear screening	350K	λ	9.5(14)	8.6(11)	8.1(10)	7.2(10)	6.0(8)	5.0(5)
			$\bar{\omega}_2$	106.7(10)	113.8(1)	115.8(7)	127.5(16)	138.0(1)	167.5(30)
ρ_m			0.38(12)	0.36(10)	0.32(10)	0.30(8)	0.29(11)	0.24(9)	
450K		λ	7.6(13)	7.4(10)	6.6(8)	6.0(10)	5.2(6)	4.4(4)	
		$\bar{\omega}_2$	119.9(11)	117.8(4)	135.8(3)	144.6(19)	157.1(6)	176.3(12)	
		ρ_m	-0.11(11)	-0.13(9)	-0.14(8)	-0.11(9)	-0.14(7)	-0.15(6)	
		T_c	428(24)	423(19)	420(19)	424(22)	418(19)	411(17)	

^aWe recalculate the LSA results. They are slightly different from those presented in Ref. [18] but within the error bars. The numerical differences are due to different settings in analyzing the PIMD data.

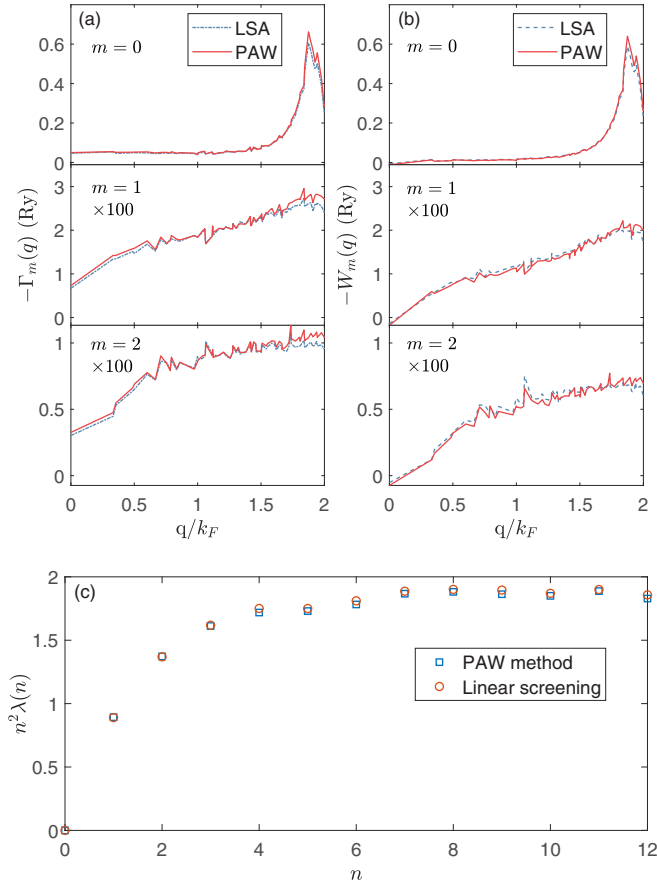


FIG. 2. Comparison between the full DFT-based implementation (PAW method) and the LSA in (a) pair-scattering amplitude $\Gamma_m(q)$, (b) effective pair interaction $W_m(q)$, and (c) interaction parameters $\lambda(n)$. The results are for $T = 450$ K and $P = 500$ GPa. $\Gamma_m(q)$ and $W_m(q)$ are obtained by recasting the matrix elements of Γ and W as a function of $q = |\mathbf{k}_1 - \mathbf{k}_2|$ for $\mathbf{k}_1, \mathbf{k}_2$ in $0.8k_F \leq |\mathbf{k}_1|, |\mathbf{k}_2| \leq 1.14k_F$.

summarized in Table I. For comparison, the LSA results are also shown. We find that the results coincide well with the LSA results. It confirms Liu *et al.*'s prediction that the superconducting transition temperature of metallic hydrogen is higher than its predicted melting temperature [18]. We note that our prediction of T_c is only valid for the liquid phase. T_c for the solid phase of metallic hydrogen had been thoroughly studied in Ref. [6].

In Fig. 2, we show the comparison of the pair-scattering amplitude $\Gamma_m(q)$ and the effective pairing interaction $W_m(q, \nu)$ between the two implementations for $P = 700$ GPa and $T = 450$ K. We find that the results yielded by the two implementations are very close. We also show the interaction parameters $\lambda(n)$ in Fig. 2(c). To determine $\lambda(n)$, we recast the matrix element $W_{11'}$ as a function of $q = |\mathbf{k} - \mathbf{k}'|$ for $0.8k_F \leq |\mathbf{k}|, |\mathbf{k}'| \leq 1.14k_F$ and evaluate Eq. (3) by integrating over q [4]. It is evident that the results also coincide well. It is not surprising that the LSA can work well in metallic hydrogen systems because hydrogen has no inner-core electron and the effective KS potential is dominated by its local part which can be well approximated by the LSA with an appropriate dielectric function. For more general systems like hydrides, the LSA is obviously inadequate, and our implementation based on the standard first-principles approach will be useful.

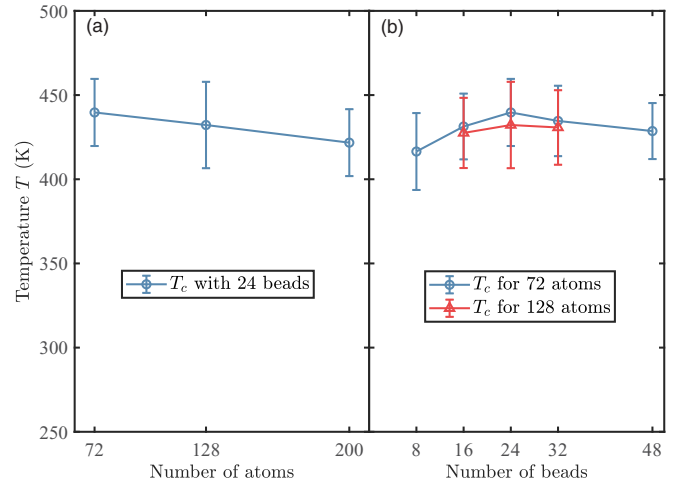


FIG. 3. Dependence of T_c on (a) different numbers of atoms and (b) different numbers of beads for $P = 700$ GPa. The error bars indicate the numerical uncertainties of the estimations of T_c 's, i.e., the values shown in parentheses in Table I.

We test the convergence of our calculation by varying the size of the simulation supercell and the number of beads discretizing the imaginary time. In Ref. [18] and the calculation shown above, we use a supercell with 200 hydrogen atoms and discretize the imaginary time to 24 beads. In Fig. 3(a), we show the dependence of estimated T_c on the number of atoms. We find that T_c slightly decreases with the increasing simulation size, but the difference is within the error bars. In Fig. 3(b), we show the dependence of estimated T_c on the number of beads. We find that only a relatively small number of beads (>16) is needed to get a converged result. The oversampling procedure discussed in Sec. II B is effective in eliminating the discretization errors.

V. SUMMARY

In summary, we present a full DFT-based implementation of the stochastic path-integral approach for estimating superconducting transition temperatures. We derive the formulas for determining the Green's function and the scattering \mathcal{T} matrix in the pseudobasis of the PAW method. Properly calculating the S matrix elements to eliminate the error due to the incompleteness of the basis is also discussed. We test our implementation in metallic hydrogen liquid systems and get results close to the those obtained in Ref. [18]. The calculation is in agreement with Liu *et al.*'s prediction and suggests that metallic hydrogen could be a superconducting liquid as its superconducting T_c is higher than the predicted melting temperature of metallic hydrogen. With the full DFT-based implementation, it becomes possible to apply the stochastic path-integral approach to a wider class of systems such as hydrides.

ACKNOWLEDGMENTS

This work is supported by the National Basic Research Program of China (973 Program) Grants No. 2018YFA0305603 and No. 2015CB921101 and the National Science Foundation of China Grant No. 11325416.

- [1] D. Duan, Y. Liu, F. Tian, D. Li, X. Huang, Z. Zhao, H. Yu, B. Liu, W. Tian, and T. Cui, *Sci. Rep.* **4**, 6968 (2014).
- [2] H. Liu, I. I. Naumov, R. Hoffmann, N. Ashcroft, and R. J. Hemley, *Proc. Natl. Acad. Sci. USA* **114**, 6990 (2017).
- [3] N. W. Ashcroft, *Phys. Rev. Lett.* **21**, 1748 (1968).
- [4] J. E. Jaffe and N. W. Ashcroft, *Phys. Rev. B* **23**, 6176 (1981).
- [5] C. F. Richardson and N. W. Ashcroft, *Phys. Rev. Lett.* **78**, 118 (1997).
- [6] J. M. McMahon and D. M. Ceperley, *Phys. Rev. B* **84**, 144515 (2011).
- [7] D. Y. Kim, R. H. Scheicher, C. J. Pickard, R. J. Needs, and R. Ahuja, *Phys. Rev. Lett.* **107**, 117002 (2011).
- [8] J. A. Flores-Livas, M. Amsler, C. Heil, A. Sanna, L. Boeri, G. Profeta, C. Wolverton, S. Goedecker, and E. K. U. Gross, *Phys. Rev. B* **93**, 020508(R) (2016).
- [9] Y. Sun, J. Lv, Y. Xie, H. Liu, and Y. Ma, *Phys. Rev. Lett.* **123**, 097001 (2019).
- [10] G. Grimvall, *The Electron-Phonon Interaction in Metals* (North Holland, 1981).
- [11] F. Giustino, *Rev. Mod. Phys.* **89**, 015003 (2017).
- [12] I. Errea, M. Calandra, C. J. Pickard, J. Nelson, R. J. Needs, Y. Li, H. Liu, Y. Zhang, Y. Ma, and F. Mauri, *Phys. Rev. Lett.* **114**, 157004 (2015).
- [13] H. Liu, I. I. Naumov, Z. M. Geballe, M. Somayazulu, J. S. Tse, and R. J. Hemley, *Phys. Rev. B* **98**, 100102(R) (2018).
- [14] J. Chen, X.-Z. Li, Q. Zhang, M. I. J. Probert, C. J. Pickard, R. J. Needs, A. Michaelides, and E. Wang, *Nat. Commun.* **4**, 2064 (2013).
- [15] H. Y. Geng, R. Hoffmann, and Q. Wu, *Phys. Rev. B* **92**, 104103 (2015).
- [16] I. Errea, M. Calandra, and F. Mauri, *Phys. Rev. B* **89**, 064302 (2014).
- [17] I. Errea, F. Belli, L. Monacelli, A. Sanna, T. Koretsune, T. Tadano, R. Bianco, M. Calandra, R. Arita, F. Mauri, and J. A. Flores-Livas, *Nature (London)* **578**, 66 (2020).
- [18] H. Liu, Y. Yuan, D. Liu, X.-Z. Li, and J. Shi, *Phys. Rev. Research* **2**, 013340 (2020).
- [19] D. Marx and M. Parrinello, *J. Chem. Phys.* **104**, 4077 (1996).
- [20] G. Kresse and J. Furthmüller, *Comput. Mat. Sci.* **6**, 15 (1996).
- [21] G. Kresse and J. Furthmüller, *Phys. Rev. B* **54**, 11169 (1996).
- [22] P. E. Blöchl, *Phys. Rev. B* **50**, 17953 (1994).
- [23] G. Kresse and D. Joubert, *Phys. Rev. B* **59**, 1758 (1999).
- [24] P. Morel and P. W. Anderson, *Phys. Rev.* **125**, 1263 (1962).
- [25] K. Knorr and N. Barth, *Solid State Commun.* **8**, 1085 (1970).
- [26] G. Bergmann, *Phys. Rev. B* **3**, 3797 (1971).
- [27] E. K. U. Gross and S. Kurth, *Int. J. Quant. Chem.* **40**, 289 (1991).
- [28] M. Lüders, M. A. L. Marques, N. N. Lathiotakis, A. Floris, G. Profeta, L. Fast, A. Continenza, S. Massidda, and E. K. U. Gross, *Phys. Rev. B* **72**, 024545 (2005).
- [29] M. A. L. Marques, M. Lüders, N. N. Lathiotakis, G. Profeta, A. Floris, L. Fast, A. Continenza, E. K. U. Gross, and S. Massidda, *Phys. Rev. B* **72**, 024546 (2005).
- [30] D. Chandler and P. G. Wolynes, *J. Chem. Phys.* **74**, 4078 (1981).
- [31] J. W. Negele and H. Orland, *Quantum Many-Particle Systems* (Addison-Wesley, 1988).
- [32] G. Giuliani and G. Vignale, *Quantum Theory of the Electron Liquid* (Cambridge University Press, 2005).
- [33] S. Ichimaru and K. Utsumi, *Phys. Rev. B* **24**, 7385 (1981).
- [34] M. Hacene, A. Anciaux-Sedrakian, X. Rozanska, D. Klahr, T. Guignon, and P. Fleurat-Lessard, *J. Comput. Chem.* **33**, 2581 (2012).
- [35] M. Hutchinson and M. Widom, *Comput. Phys. Commun.* **183**, 1422 (2012).
- [36] J. P. Perdew, K. Burke, and M. Ernzerhof, *Phys. Rev. Lett.* **77**, 3865 (1996).